Pointing Stability Performance of the Cassini Spacecraft

Allan Y. Lee* and Emily L. Burrough†
Jet Propulsion Laboratory, California Institute of Technology

Twelve scientific instruments onboard the Cassini spacecraft depend on the accurate pointing capabilities of the spacecraft to return data critical to the success of the mission and to improving our understanding of Saturn. Throughout the seven year interplanetary cruise to Saturn and the four year prime mission, the control of the Cassini spacecraft is achieved by employing either the Reaction Control System (RCS) composed of a set of eight thrusters or the Reaction Wheel Assembly (RWA) made up of four reaction wheels, only three of which are active at a given time. The operations of Cassini imaging instruments (such as the Narrow Angle Camera) require a high level of spacecraft pointing stability in order to minimize the distortion and smearing of the image during the exposure time. In designing the Cassini attitude control system, a pointing stability performance metric that considered the frequency contents of the disturbance sources was employed. The flight performance of the Cassini pointing stability, achieved with a set of three reaction wheels or RCS thrusters, is summarized in this paper.

Acronyms

AACS	=	Attitude and Articulation Control Subsystem
BOB	=	Bang Off Bang (Thruster Controller)
B/S	=	Bore-sight Vector
BW	=	Bandwidth (of a Controller)
DOY	=	Day of Year
FOV	=	Field Of View
GWE	=	Gravity Wave Experiment
IRU	=	Inertial Reference Unit
JPL	=	Jet Propulsion Laboratory
NAC	=	Narrow Angle Camera
PMD	=	Propellant Management Device
PSD	=	Power Spectral Density
RCS	=	Reaction Control System
RMS	=	Root Mean Squares
RPWS	=	Radio and Plasma Wave Science
RWA	=	Reaction Wheel Assembly
S/C	=	Spacecraft
SCO	=	Spacecraft Operations
SOI	=	Saturn Orbit Insertion
SRU	=	Stellar Reference Unit (Star Tracker)

I.Cassini/Huygens Mission to Saturn/Titan

The Cassini orbiter is a platform for exploration, home to twelve scientific instruments sent on a seven year, 1.5 billion km journey to discover Saturn. As the four year primary mission nears a conclusion in July of 2008, the value derived from Cassini will continue be discussed in scientific circles for years to come. Major science

*Project Element Manager, Attitude and Articulation Control System, Cassini Spacecraft Operations Office. Mail Stop 230-104, Jet Propulsion Laboratory, 4800 Oak Grove Drive, Pasadena, California 91109-8099, USA. Allan.Y.Lee@jpl.nasa.gov
†Uplink Engineer, Attitude and Articulation Control System, Cassini Spacecraft Operations Office. Mail Stop 230-104, Jet Propulsion Laboratory, 4800 Oak Grove Drive, Pasadena, California 91109-8099, USA. Emily.L.Burrough@jpl.nasa.gov

objectives of the Cassini mission include an investigation of the configuration and dynamics of Saturn's magnetosphere, the structure and composition of the rings, the characterization of several of Saturn's icy satellites, and the constituent abundance of the atmosphere of Titan.[1] Additionally, Doppler tracking experiments using the Earth and the Cassini spacecraft as separated test masses are conducting gravitational wave searches.[2] A highlight of the Cassini mission was the discovery of a plume of water ice and other gases originating from the south pole of the icy moon Enceladus. Cassini also served as transport to the European Space Agency's Huygens Probe, sent to characterize the surface of Saturn's largest moon, Titan.[3,4]

The Spacecraft Operations Office (SCO) at the Jet Propulsion Laboratory (JPL) focuses on protecting this scientific platform from the harsh space environment to ensure the reliability of the spacecraft's components on which the science return depends. A group within SCO, the Attitude Articulation and Control Subsystem (AACS), is tasked with guaranteeing that the pointing designs of each instrument execute safely and successfully onboard the spacecraft. The Cassini AACS estimates and controls the attitude of the three-axis stabilized Cassini spacecraft as it responds to ground-commanded pointing goals for the spacecraft's science instruments. To achieve the commanded targets within the required accuracy, AACS uses either thrusters or reaction wheels to control the spacecraft. The AACS also executes ground-commanded spacecraft velocity changes. To this end, AACS uses either a rocket engine or a set of Z-facing thrusters to effect a velocity change. To achieve a high degree of maneuverability and to facilitate high-resolution camera imaging, Cassini is designed as a three-axis stabilized spacecraft.[4] Attitude determination sensors used by Cassini AACS include two Stellar Reference Units (SRU), two Sun Sensor Assemblies (SSA), and two Inertial Reference Units (IRU).

This paper will characterize Cassini's pointing stability from data collected during the prime tour operations while the spacecraft is controlled by either the RWA or the RCS. Pointing stability is defined as the time-varying effects on science instrument pointing caused by the dynamic interactions between spacecraft structure and mechanisms, attitude control and determination errors, structural thermal distortion, and other environmental disturbances. Since Cassini's launch on October 15, 1997, spacecraft attitude is routinely estimated on-board and telemetered to SCO. However, to date, the pointing stability performance of the Cassini AACS design has only been confirmed indirectly. In an email sent to the authors of this paper, the principal investigator of the Imaging Science team stated that "*From all I have seen, the AACS guys have a lot to be proud of. You have given us a remarkable platform from which to take pictures*." This paper documents our effort to better characterize and understand the pointing stability performance of the Cassini spacecraft over the span of the prime mission.

A.Spacecraft Configuration

A sophisticated interplanetary spacecraft, Cassini is one of the largest spacecraft humans have ever built and launched. The orbiter is about 6.8 m in height with a "diameter" of 4 meters. The total mass of the spacecraft at launch was approximately 5574 kg, which includes about 3000 kg of bi-propellant (1869 kg of Nitrogen Tetroxide, and 1131 kg of mono-methyl hydrazine), 132 kg of high purity hydrazine, and 2442 kg of "dry" mass (including the 320-kg Huygens Probe and 9 kg of helium mass). Cassini is a flexible spacecraft containing four structural appendages and three propellant tanks. The four appendages are the 11-meter long magnetometer boom and three similar Radio and Plasma Wave Science (RPWS) antennas. The fundamental frequency of the magnetometer boom is 0.67 Hz, and its damping ratio is between 0.2 and 1% (depending on the size of the boom deflection). Its second mode frequency is 4 Hz. The RPWS antennas have a fundamental frequency of 0.13 Hz and a damping ratio of 0.2%. Its second mode frequency is 0.86 Hz.

The propulsion module houses two cylindrical tanks with hemispherical end domes. These tanks each contain an eight-panel Propellant Management Device (PMD) of the surface tension type. These PMDs are used to control the orientation of the propellant in the low-g environment via surface tension forces. The monopropellant (hydrazine) is kept in a spherical tank that is located off the Z-axis. The tank contains an elastomeric diaphragm for bubble-free expulsion of hydrazine in micro-g condition. The total mass of the hydrazine at launch was about 132 kg.

When the spacecraft attitude is controlled by a set of three reaction wheels or eight thrusters, the bipropellant is in a so-called "low-g" sloshing mode. In this mode, surface tension forces control the motion of the propellant inside the tanks. The propellant will assume a shape determined by surface tension forces and the geometry of the PMD. At a 50% fill fraction condition, the monomethyl hydrazine/nitrogen tetraoxide (MMH/NTO) fuel sloshing frequencies are estimated to be 2-4 mHz.[6] At fillfractions that are higher or lower than 50%, the sloshing frequencies are higher. For example, at a fill fraction of 20%, the estimated frequencies are 3-5 mHz. At a fill fraction of 70%, the estimated frequencies are 4-6 mHz. However, the uncertainties associated with these frequency estimates are large. The damping ratio of the fuel sloshing motion in the 'low-g" mode is estimated to be 10%.

When the spacecraft experiences "high" acceleration due to the firing of a rocket engine (with a nominal thrust of 445 N), the bi-propellant settled to the "bottom" of the tanks with a "flat" surface that is perpendicular to the thrust vector of the engine. For the purpose of thrust vector control, two gimbal actuators are used to articulate the main engine thrust. This introduces lateral acceleration disturbances. Propellant responds by forming standing waves on the "free" surface, which is called "sloshing". In this "rocket firing" scenario, the sloshing motions of the bipropellant in the tanks are in a so-called "high-g" mode. During a main engine burn with the tanks at about 50% fill fraction condition, the fuel-sloshing frequency is estimated to be 0.05-0.14 Hz. The estimated damping ratio of the fuel sloshing motion was 10-35%.[6] Key frequencies of the Cassini structure and instruments are depicted in Fig. 1.

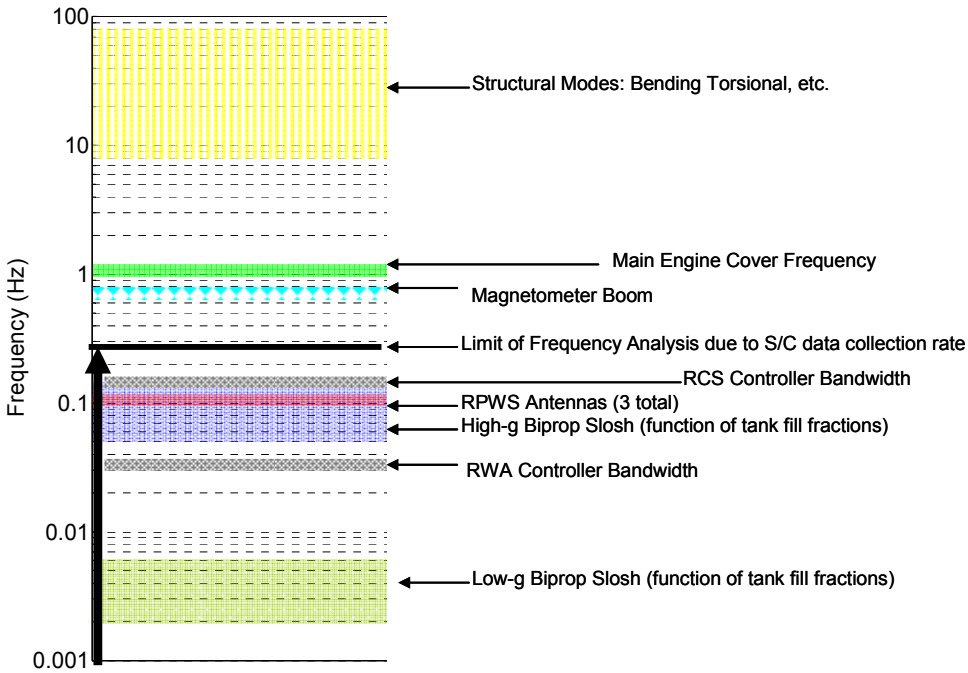

Figure 1. Fundamental frequencies of the Cassini spacecraft and instruments.

B. Attitude Control by either Reaction Wheels or RCS Thrusters

A high level of spacecraft pointing stability is needed during imaging operations of high-resolution science instruments such as the Narrow Angle Camera (NAC). Typically, the required level of pointing stability is not achievable with an orbiter controlled by thrusters. Instead, three Reaction Wheel Assemblies (RWAs) are employed to suit this purpose. Cassini carries a set of three "strap-down" reaction wheels that are mounted on the lower equipment module. The RWAs are oriented "equal distance" from the spacecraft's Z-axis with a backup reaction wheel mounted on top of an articulatable platform.[5,7,8]

1. Cassini RWAController Design[7]

The Reaction Wheel Assemblies (RWAs) are used primarily for attitude control when precise and stable pointing of a science instrument (such as NAC) is required during the prime mission phase. To this end, RWAs are used to slew the spacecraft from one attitude to another, rest to rest. Once it has arrived at the targeted attitude, the NAC "stares" at the target for a period of time (the "exposure" time of the NAC) during which the spacecraft attitude must be stable. As a requirement, the Reaction Wheel Attitude Control System (RWAC) must control the spacecraft with per-axis attitude control errors that are smaller than 40 μrad. While under reaction wheel control, the spacecraft pointing stability must be better than those specified in Table 1. Because the spacecraft's principle axes are very closely aligned with the spacecraft's mechanical axes, the basic structure of the RWAC is a decoupled, three-axis, Proportional and Derivative (PD) controller. Due to the presence of bearing frictional torque in the reaction wheels, a controller with the "PD" control architecture will not be able to drive the spacecraft attitude control error to zero unless an integral term is added to the PD controller. This difficulty was overcome by the

addition of a Proportional and Integral (PI) estimator of the reaction wheel frictional torque in the reaction wheel "Hardware Manager." In effect, integral control action is added "locally" to remove any steady-state spacecraft's attitude control errors. The RWAC design has a bandwidth of 0.0299 Hz.[7] As depicted in Fig. 1, a RWAC with this bandwidth will not excite structural modes, but will be able to arrest low-g fuel sloshing vibratory motions.

The RWAC was first used on March 16, 2000, several months ahead of the start of the Jupiter campaign. During the Jupiter campaign, the Approach Science (January to June, 2004), and at the start of the prime mission, the following per-axis slew rates and accelerations were used to slew the spacecraft using the reaction wheels: [1.65, 1.78, 3.08] mrad/s and [9, 10, 17] μrad/s^2 about the spacecraft's X, Y, and Z-axis, respectively. These slew profile limits were selected to be consistent with the capabilities of the reaction wheel torque and momentum storage capacity. They were also selected assuming at least 90 W of power is allocated for the three reaction wheels. The Huygens Probe was successfully released on December 24, 2004. There was a corresponding drop in the moments of inertia of spacecraft after the Probe release. As such, the slew profile limits were raised in early 2005 to [1.92, 2.30, 3.90] mrad/s and [10, 13, 22] μrad/s^2 about the spacecraft's X, Y, and Z-axis, respectively.

2. Cassini RCS Controller Design[7]

A conventional Bang-Off-Bang (BOB) thruster control algorithm is used by Cassini AACS. The BOB algorithm uses error signals that are the weighted sums of per-axis attitude errors and attitude rate errors to control thruster firings. But such a control algorithm can result in "two-sided" limit cycles that waste both hydrazine and thruster on/off cycle. To counter these drawbacks, the Cassini's BOB incorporated a "self-learning" feature to produce, as much as possible, "one-sided" limit cycles in the presence of small environmental torque. In this scheme, an "optimal" thruster pulse is fired to send the spacecraft attitude control error signal towards the other side of the dead-band. The pulse is adaptively adjusted so that it will get close to the dead-band space but without "touching" it. The resultant "one-sided" limit cycles save both hydrazine and thruster on/off cycle.

The spacecraft's attitude control errors while on thruster control are "command-able" via a "7DEADBAND" command. The three arguments of this command provide the flight software with the magnitudes of the one-sided dead-band about the spacecraft's X, Y, and Z-axis. During early Cruise with the HGA pointed at Earth for X-band communication, dead-band of [2, 2, 20] mrad was used to assure that the inertial pointing control requirement for X-band downlink was met. At times when accurate pointing was not needed, AACS used dead-band of [20, 20, 20] mrad in order to save both hydrazine and thruster on/off cycle. On the other hand, the attitude control dead-band was tightened to [2, 2, 2] or even [0.5, 0.5, 0.5] mrad to satisfy Science pointing requirements.

Undesirable interactions between thruster firings and the 0.67-Hz magnetometer boom might occur during main engine burns or low-altitude Titan flybys. To avoid these interactions, 2nd order notch filters (with a notch frequency of 0.7 Hz) are used to filter both the attitude and attitude rate control error signals before they are fed to the RCS controller. The bandwidth of the RCS attitude controller is selected to be 0.15 Hz, which is significantly higher than the low-g bi-propellant sloshing frequencies (2-4 mHz at 50% tank fill fraction).[6] The minimum impulse bit of these thrusters is on the order of 7-8 milli-seconds.[10]

From the spacecraft's launch in 1997 through 2003, Cassini predominately used a set of eight thrusters to control the spacecraft's attitude. During Tour, the spacecraft was slewed mainly using three prime reaction wheels. Thrusters are only used to control the spacecraft's attitude during low-altitude Titan flybys, biasing the reaction wheels' angular momentum vectors, and to perform small ΔV maneuvers.

II. Pointing Control and Stability Requirements

Spacecraft pointing control is defined by the angle between the actual pointing direction and the desired pointing direction of a particular on-board body vector. The S/C pointing control requirement is driven by the need to guarantee that the selected science target falls inside the FOV of the science instrument. If the 2 mrad (radial 99%) pointing control requirement is met, the captured image is guarantee to fall inside the 6.1×6.1 mrad FOV of the NAC.

Spacecraft pointing stability is defined by the angle variation of the actual pointing direction of an on-board body vector over a time duration named exposure time (or dwell time or frame time). The S/C pointing stability requirement is driven by the need to ascertain that over the exposure time of the camera, incoming photons are "focused" on the intended set of camera CCD pixels. If the instrument moves during the exposure time, photons will fall on that set of pixel as well as neighboring pixels, and a fuzzy image results. The specific pointing stability requirement selected corresponds to a tolerable degradation of image quality.

A. Science Driven Pointing Requirements

Cassini carries twelve scientific instruments, half of which are considered remote sensing instruments based on the objects which they observe. The six remote sensing instruments on Cassini are:

(1) Imaging Science Subsystem (ISS)
(2) Visible and Infrared Mapping Spectrometer (VIMS)
(3) Composite Infrared Spectrometer (CIRS)
(4) Ultraviolet Imaging Spectrograph (UVIS)
(5) Cassini Radar (RADAR)
(6) Radio Science Subsystem (RSS)

The first four of these instruments are mounted and co-aligned on the remote sensing pallet. Also mounted on the remote sensing pallet are two redundant stellar reference units (star trackers). The ISS consists of two cameras: Narrow Angle Camera (NAC) and the Wide Angle Camera (WAC). The Field of View (FOV) of the NAC is 6.1×6.1 mrad (±3.05 mrads). That of the WAC is 61.2×61.2 mrad. The NAC bore-sight vector is nominally aligned with the minus Y-axis of the spacecraft. The FOV of CIRS is ϕ3.9 mrad (for Focal Plane-1, FP1). Its FOV for FP3 and FP4 is 0.3×2.9 mrad. The FOV of UVIS (narrow) is 0.75×61 mrad. The FOV of UVIS (wide) is 8×61 mrad. The FOV of VIMS is 32×32 mrad. With FOV of only several mrads, the inertial pointing of these instruments must be made with great care. Key science pointing control and stability requirements for the Cassini spacecraft are given in Table 1.[5]

Table 1. Cassini Science Pointing Control and Stability Requirements

Pointing Requirements	Requirements	Remarks
Science inertial pointing requirements (radial 99%)	(mrad)	Applicable only
Control	2.0	when S/C is
Knowledge	1.0	quiescent
Science pointing stability requirements (2σ per axis) for time windows of:[5,11]	(μrad)	
0.5 s	4	ISS, VIMS
1 s	8	ISS, VIMS
5 s	36	CIRS
22 s	100	CIRS
100 s	160	ISS, VIMS, CIRS
900 s	200	VIMS
1200 s	220	ISS
1 hour	280	UVIS
(Applicable 20 s after a rest-to-rest S/C slew while the S/C is quiescent)		

These tight S/C pointing requirements are met by the Cassini attitude control subsystem. Further comparison of actual flight performance to the design requirements listed in Table 1 will be provided in Section IV as proof to this assertion. The spacecraft's three-axis attitude is estimated using measurements from both the IRUs and the SRUs. Three Reaction Wheel Assemblies (RWAs) are used to control the S/C base-body. In Appendix A, Table A1 is the flight performance of the spacecraft pointing control performance. In this table, component errors are "summed" to form a RSS (Root Sum Squares) sub-total. The overall spacecraft pointing capabilities are then determined assuming that the two per-axis capabilities are fully correlated and have Gaussian probabilistic distributions. Obviously, the inertial pointing control requirement is met with margins. In Appendix A, Table A2 is the flight performance of the spacecraft pointing knowledge performance.

B. Sources of Spacecraft Pointing Jitter

Spacecraft jitter control is effective only when the causes of jitter are well understood. The following sources (in random order) of jitter are applicable to Cassini:

(1) Reaction wheels' imperfections. The static imbalance of a RWA generates a rotating force that is proportional to the squared spin rate of the wheel. This force in turn generates a torque about the spacecraft's center of mass. Similarly, the dynamic imbalance generates a rotating torque that is proportional to the squared spin rate of the wheel. Other disturbance sources due to RWA operations include bearing viscous drag torque, random drag torque spikes, the finite size of the least significant bit of the formatted torque commands and computation torque ripple.

(2) Structural dynamics. The flexibility of the Cassini spacecraft is described in Section I. The fundamental frequency of the magnetometer boom is 0.67 Hz (its second mode frequency is 4 Hz). The RPWS antennas have a fundamental frequency of 0.13 Hz (its second mode frequency is 0.86 Hz). The bandwidth of the RWA controller is 0.03 Hz. As such, RWA control actions will not excite either the Magnetometer of RPWS structural modes. Other than these flexible modes, finite element modeling of the Cassini main structures revealed other higher frequency structural modes. The fundamental set of frequencies is [7.36, 7.70, 15.76] Hz (bending, bending, torsion), and there are another 112 modes below 79 Hz.

(3) Low-g fuel sloshing Motion. The dynamics of low-g fuel sloshing motion is also described in Section I. At fill fractions of 20%, 50%, and 70%, the MMH/NTO fuel sloshing frequencies are estimated to be 3-5, 2-4, and 4-6 mHz, respectively. However, the uncertainties associated with these frequency estimates are significant. Near the end of the Cassini prime mission (July 1, 2008), the fill fractions of these tanks are estimated to be lower than 14%.

(4) Slew-induced structural vibration. When a S/C is slewed from one inertial attitude to another, residual structural vibration after the completion of the slew might be significant. The magnitude of these residual vibrations is related to both the natural frequencies (Ω) and damping ratios (ς) of the major spacecraft structural and sloshing modes. They are also related to the magnitude of angular acceleration (α_{slew}) used in slewing the S/C, as well as the elapsed time between the end of the slew and the time at which science observations is to begin (sometime it is called slew settling time, T_s). In general, the magnitude of the residual vibratory S/C attitude after a slew is bounded by: $\alpha_{slew} Q \times e^{-\varsigma\Omega T_s} / \Omega^2$.[12] Here, Q is related to the inertia properties of both the S/C and the flexible bodies (e.g., magnetometer boom).

(5) Sensor noise with a significant frequency content within the controller bandwidth looks like valid "command" to the attitude controller. Accordingly, the controller will generate control torque in order to cause the S/C attitude to follow these erroneous "commands." This results in undesired S/C motion. Gyroscope-related noises include quantization error, angle random walk, and rate random walk.

(6) Articulation mechanisms. The Cosmic Dust Analyzer measures flux, velocity, charge, mass, and composition of dust and ice particles in the mass range of 10^{-16} to 10^{-6} grams. It has two types of sensors: high rate detectors and a dust analyzer. An articulation mechanism permits these sensors to be rotated to several positions relative to the orbiter. Articulation motions impart disturbance torque on the base body of the spacecraft. Additionally, the NAC has 24 filter wheels which can impart disturbance torque on the base body when changed.

(7) Environmental disturbance torque. During a low-altitude flyby of Titan, the spacecraft will experience significant aerodynamic torque due to the Titan atmosphere. Similarly, during a low-altitude flyby of Enceladus, the spacecraft will experience disturbance torque due to the watery plume clouds. This torque must be countered by frequent thruster firings, and the corresponding S/C motion will be very jittery. Other environmental torque includes solar radiation torque, power generator radiation torque, and gravity gradient torque.

(8) Thermal gradient caused by re-orientation of the spacecraft base body will cause thermal/mechanical snaps, creep strain relief "popping" (structural annealing), and micro stick-slip at loaded mechanical joints.

Other disturbance sources that are not applicable to Cassini include the reaction torque that is imparted on the spacecraft base body due to vibratory motions of the flexible solar panels, reaction torque due to antenna pointing and tracking motion, as well as excitation due to tape recorder motions.

III. Spacecraft Pointing Stability

There are several potential sources for instability of spacecraft pointing, but in order to qualitatively discuss these causes, one first must be able to measure the effects on spacecraft motion. The following section discusses two methods to quantify pointing stability, the "peak-to-peak" and the "root mean square (RMS)" method for calculating pointing stability. Both methods are applied to a test case from the Cassini prime mission and the results used to refine further analysis of the spacecraft telemetry.

A. Methods of Defining Pointing Stability of Spacecraft Motions

A so-called "peak-to-peak" pointing stability metric is commonly used to specify the level of motion stability of the line-of-sight (LOS) of an on-board instrument. This method was used, for example, on both the two Voyager missions and the Mars Pathfinder missions. Let $\phi(t)$ be the time history of the angular displacement of the instrument LOS. Let T be the dwell time (or exposure time) of the instrument. The windowed peak stability of the motion, from time t to t+T, is defined by $s_P(t,T)$. The peak stability of $\phi(t)$ for an exposure time of T, denoted by $\sigma_{SP}(T)$, is defined as the square root of the expected value of squared $s_P(t,T)$. Mathematically, the peak-to-peak stability metric is given by:

$$\begin{aligned} &\text{Windowed Peak Stability} = s_P(t,T) = \underset{\tau\in[0,T]}{\text{Max}}\left|\phi(t+\tau)-\phi(t)\right| \\ &\text{Squared Peak Stability} = \sigma_{SP}^2(T) = \text{Expect}\{s_P^2(t,T)\} = \frac{1}{N}\sum_{t_i=t_1}^{t_i=t_N} s_P^2(t_i,T) \end{aligned} \tag{1}$$

One obvious drawback of this pointing stability metric is that it uses only the two extrema points in the time history of the pointing error that fall within a time window of interest T. Another weakness of this pointing stability metric is that the degree to which disturbances at different frequencies contribute to jitters is not captured or easily extracted using this metric. The "peak-to-peak" method was considered to be overly conservative and not sensitive enough to capture the characteristics of different disturbance frequencies on image quality. For this reason, Cassini designers adopted a new method, termed the "root mean square (RMS)" pointing stability which compares pointing stability deviations to the mean within a defined window of interest. A summary of both methods is shown below in Fig. 2.

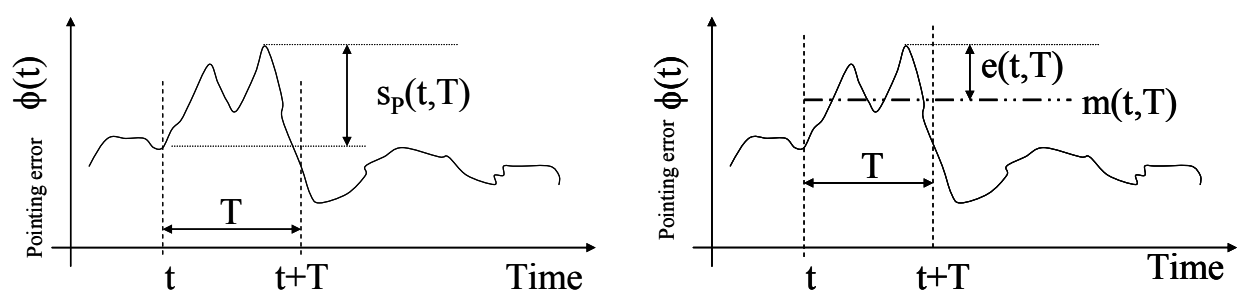

Figure 2. Representative calculation of (a) Peak-to-Peak Pointing Stability and (b) RMS Pointing Stability.

The RMS pointing stability metric, σ_{RMS}, was first introduced by Lucke, Sirlin, and San Martin,[11] and has since been adopted by both the Cassini and the Space Interferometry Mission.[12] Mathematically, the RMS stability metric is defined as follows:

$$\begin{aligned} &\text{Windowed mean} = m(t,T) = \frac{1}{T}\int_t^{t+T}\phi(\tau)\,d\tau, \\ &\text{Deviation from windowed mean} = e(\tau,t,T) = \phi(\tau) - m(t,T), \\ &\text{Windowed variance} = \sigma_W^2(t,T) = \frac{1}{T}\int_t^{t+T} e^2(\tau,t,T)\,d\tau, \\ &\text{Squared RMS Stability} = \sigma_{RMS}^2(T) = \text{Expect}\{\sigma_W^2(t,T)\} = \frac{1}{N}\sum_{t_i=t_1}^{t_i=t_N}\sigma_W^2(t_i,T) \end{aligned} \tag{2}$$

In the frequency domain, the RMS stability metric is given by:[11]

$$\sigma_{RMS}^2 = \int_0^\infty \Phi_{PSD}(f) \times W(f,T) df \tag{3}$$

Here, $\Phi_{PSD}(f)$ is the power spectral density of $\phi(t)$, in rad^2/Hz, $W(f,T) = W(C) = 1-2(1-\cos C)/C^2$ and $C = 2\pi fT$. Fig. 3 depicts how the weighting function W(C) varies with its argument C. From this figure, we note that $W \geq 0.5$ when $C \geq 2.78$. That is, for an exposure window T of 10 msec, disturbances at frequencies higher than $2.78/(2\pi\times0.01) \approx 44.2$ Hz will have a greater impact on the spacecraft pointing stability than those below that frequency. In other word, the weighting function W is a high-pass filter with a "crossover" frequency near $2.78/(2\pi T) \approx 0.442/T$ Hz (where T is in units of seconds). This mathematical result confirms our intuition that jitter in images taken with small exposure times will not be affected by "low" frequency disturbances (where "low" frequency is inversely proportional to the exposure time).

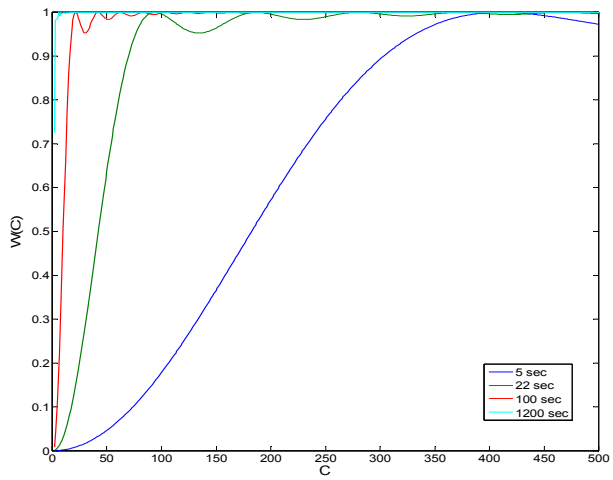

Figure 3. The Weighting Function W(C)

As an illustration, both the peak and RMS pointing stability metric were applied to a RWA-based WAC observation (from 2007-164T14:46 through 2007-164T15:45) and the results are compared in Table 2. The S/C was quiescent with all three per-axis attitude rates lower than 0.01 deg/s throughout this observation period. The approximate moments of inertia of the spacecraft at the time of this observation are [7110, 5900, 3670] kg-m^2 about the X, Y, and Z-axis, respectively. The time history of the X-axis attitude telemetry is depicted in Fig.4(a). These telemetry data are recorded at 2-s intervals. To assure good S/C pointing stability, telemetry was processed only after 200 s from the last rest-to-rest slew and the start of the WAC observation at 2007-164T14:46. The weighted power spectral density (PSD) of the X-axis time data, in log-log scale, is depicted in Fig. 4(b). The PSD data are computed using a Matlab program that processes the raw telemetry according to the window intervals of interest. In this case, the window durations of [5 22 100 1200] seconds were selected in order to better compare the spacecraft's performance to the requirements defined during the spacecraft design and development phase. Finally, the cumulating pointing stability versus frequency is shown in Fig. 4(c) for a 22 sec exposure window.

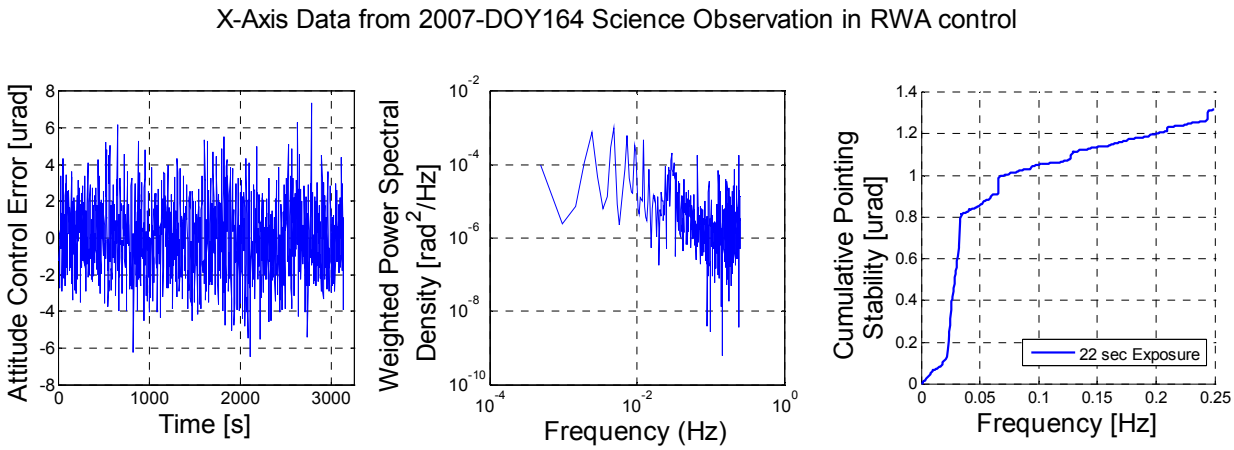

(a) **(b)** **(c)**

Figure 4. Time History of X-axis (a) Attitude Control Error , (b) the Weighted PSD Result and (c) the Cumulative Pointing Stability.

Table 2. Peak and RMS Pointing Stability Metric

S/C Axes	Peak Stability	RMS Stability	
		2σ per axis [μrads]	
	Time-domain	Time-domain	Frequency-domain
100-s Exposure Time			
X-axis	13.3	2.8	2.8
Z-axis	9.2	3.9	3.6
1200-s Exposure Time			
X-axis	8.2	2.9	2.8
Z-axis	11.6	4.1	4.0

Since this is a WAC observation, only pointing stability metric for two exposure times, 100 s and 1200 s, are compared (see Table 2). Also, since the B/S axis of WAC is nominally aligned with the S/C's Y-axis, only pointing stability metric about the X and Z-axis are of interest. From results given in Table 2, we observe that:

(1) The peak stability metric is always larger than its RMS stability metric counterpart.
(2) The pointing stability about the Z-axis is always larger than its X-axis pointing stability counterpart. This is because the S/C Z-axis moment of inertia is smaller than the X-axis moment of inertia.
(3) The actual RMS stability for exposure times of 100 and 1200 s are both at least an order of magnitude better than their respective requirements (see Table 2). This explains why images taken by the two ISS cameras are so clear.
(4) The RMS pointing stability metric are computed using the time domain approach (Eq. (2)) closely approximates that computed using the frequency domain approach (Eq. (3)). Moreover, time-domain results always bound their frequency-domain counterparts. This is because the frequency-domain results are computed using integrations whose upper limit was 0.25 Hz (instead of "infinity" from Eq. (3)).
(5) The cumulative pointing stability depicted in Fig. 4(c) shows a "sudden" improvement in stability at frequencies lower than 0.03-0.0335 Hz. This could be due to control action on the part of the RWA controller (whose BW is 0.03 Hz).

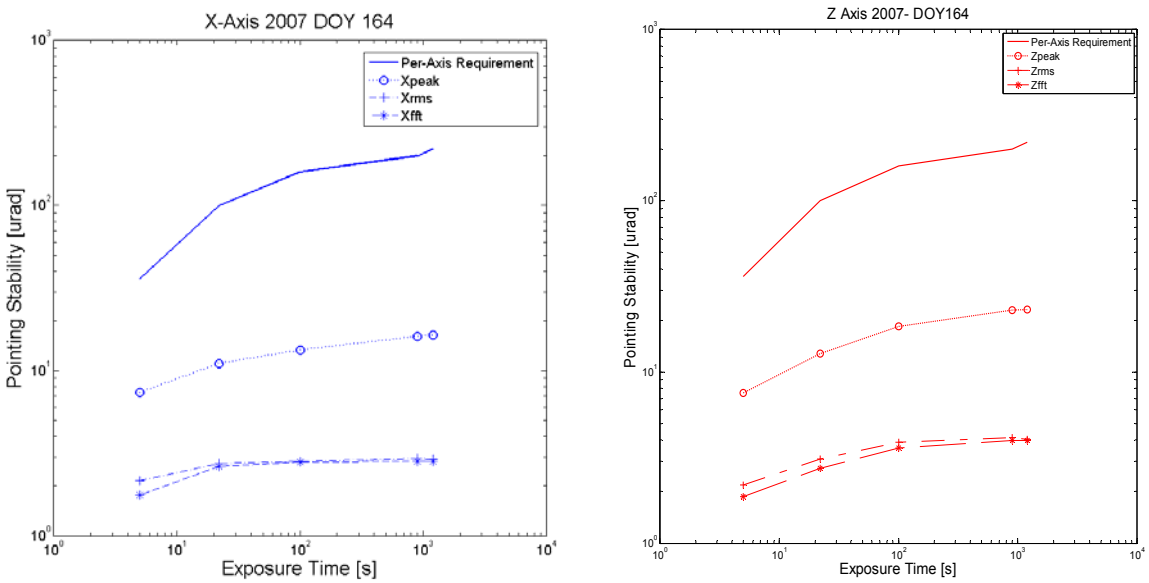

(a) **(b)**

Figure 5. "Peak-to-peak" and RMS Spacecraft Pointing Stability while in RWA control for the (a) X-Axis and (b) Z-Axis on 2007-DOY-164.

The dependencies of the X and Z-axis pointing stability performance on exposure times are depicted in Fig. 5. Superimposed on these plots are the pointing stability requirements. Results given in these figures and Table 5 both suggest that the peak-to-peak values are TBD times larger than their (1-sigma) RMS pointing stability counterparts. Obviously, this "conversion" factor is only applicable to Cassini data, but it could be used as a guide in relating pointing stability requirements that are expressed in these two performance metrics. Further analysis of Cassini telemetry in Section IV will use the RMS method to characterize the performance of the Cassini pointing stability in both RWA and RCS control modes.

IV. Spacecraft Pointing Stability Performance

The following section presents the pointing stability results from 2003 through 2008 while the spacecraft collected science in either the RCS or RWA control mode. To generate these numbers telemetry from the spacecraft was passed through a MATLAB code that calculated RMS pointing stability in both the frequency and time domain. The telemetry channels used for these calculations are the attitude control results for the X, Y and Z-axis and are recorded at intervals of two seconds. With a data collection at two second intervals our analysis of pointing stability frequency was limited to a range of 0 to 250 mHz, but even within this small frequency band interesting interactions were observed.

A. Flight Performance of Cassini RWA Pointing Stability

Flight experience indicates that the RWAC was well designed. Representative per-axis attitude control errors with the spacecraft in a quiescent state were always bounded by ±40 μrad about all the spacecraft axes. The pointing stability performance of the spacecraft is summarized in Table 3. The achieved spacecraft pointing stability easily meets the requirements specified in Table 1 with significant margin. The high quality of images returned by the high-resolution cameras provides ample evidence to this claim.

A total of ten sets of data were collected and analyzed to generate a range of Cassin's pointing stability performance from 2003 through 2008. In an effort to compare like cases the data sets were limited to time periods where all three per-axis attitude rates are lower than 0.01 deg/s throughout this observation period. Doppler tracking experiments using the Earth and the spacecraft as test masses were conducted by Cassini for gravitational wave searches in the low frequency range (10^{-4} to 10^{-3} Hz). For time periods ranging between 20 to 40 days centered about its solar opposition, the spacecraft was tracked continuously (in Ka-band, approximately 32 GHz) in the search for gravitational waves that were predicted by Einstein's general relativity theory. The third and last search was only 20 days long and was conducted over November 12, 2003 through November 30, 2003 and its pointing stability results

are included as a case study of Cassini's RWA pointing stability performance. Along with the pointing stability performance from the third Gravity Wave Experiment in late 2003, nine other cases were selected for analysis to represent a complete picture of the Cassini pointing performance over the prime mission. The other cases selected represent different point and stare science observations performed in RWA control. The results of all ten cases are summarized in Table 3 below.

Table 3. RMS Pointing Stability, 2σ per axis [μrads]

Mission Phases	Days Since Launch [days]	Exposure Time [s]			
		5	22	100	1200
		X-Axis			
2003-328	2229	1.65	2.12	2.27	2.30
2004-136	2403	1.69	2.16	2.23	2.25
2004-261	2528	1.75	2.29	2.52	2.69
2005-102	2734	1.75	2.25	2.59	2.73
2006-086	3083	1.66	2.08	2.21	2.37
2006-307	3304	1.71	2.16	2.25	2.37
2007-126	3488	1.73	2.40	2.54	2.61
2007-355	3717	1.70	2.14	2.25	2.43
2008-007	3734	1.76	2.22	2.37	2.85
2008-113	3840	1.75	2.20	2.47	2.72
		Y-Axis			
2003-328	2228	1.46	1.88	2.04	2.06
2004-136	2403	1.65	2.51	2.60	2.62
2004-261	2528	1.52	1.92	2.02	2.05
2005-102	2734	1.54	1.94	2.08	2.10
2006-086	3083	1.53	1.88	2.03	2.07
2006-307	3304	1.57	1.98	2.11	2.14
2007-126	3488	1.56	2.19	2.47	2.56
2007-355	3717	1.59	2.16	2.29	2.34
2008-007	3734	1.58	1.98	2.12	2.18
2008-113	3840	1.56	1.97	2.11	2.15
		Z-Axis			
2003-328	2228	1.68	2.19	2.33	2.35
2004-136	2403	1.84	2.44	2.89	3.12
2004-261	2528	1.81	2.39	2.51	3.52
2005-102	2734	1.78	2.36	2.62	2.65
2006-086	3083	1.79	2.41	2.36	3.82
2006-307	3304	1.84	2.42	3.01	3.29
2007-126	3488	1.84	2.54	3.40	3.84
2007-355	3717	1.83	2.40	3.29	3.75
2008-007	3734	1.77	2.36	3.28	3.73
2008-113	3840	1.82	2.42	3.37	3.82

These data points overwhelming confirm that the Cassini pointing performance while in RWA control is significantly better than the science-driven requirements throughout the prime mission. The pointing stability of the spacecraft does not degrade substantially over the life of the prime mission. Even as the mass properties of the spacecraft underwent a significant decrease after Saturn Orbit Insertion (Δ mass= 850 kg on 2004-DOY183) and the release the probe (Δ mass = 320 kg on 2004-DOY360). The dependency of the spacecraft pointing stability on exposure time, in log-log scale, is depicted in Fig. 6. Superimposed on these plots is the pointing stability requirement curve based on data from Table 1.

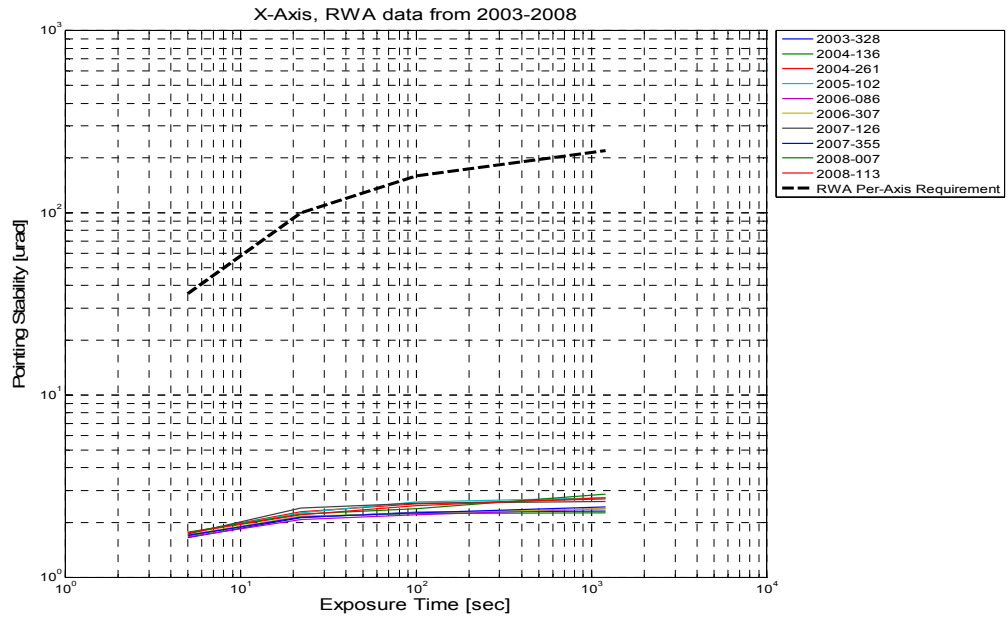

Figure 6. Summary of Spacecraft Pointing Stability (RMS method, 2-sigma) while in RWA-control from 2003-2008 for the X-Axis.

For each of the ten cases listed above, the cumulative pointing stability versus frequency was analyzed to determine the sources of pointing stability based on known fundamental frequencies of the spacecraft's instruments and structure. The results are presented below in Figs. 7 and 8 for each axis over various exposure times [5 22 100 1200 sec] for the GWE-3 that began on 2003-DOY328.

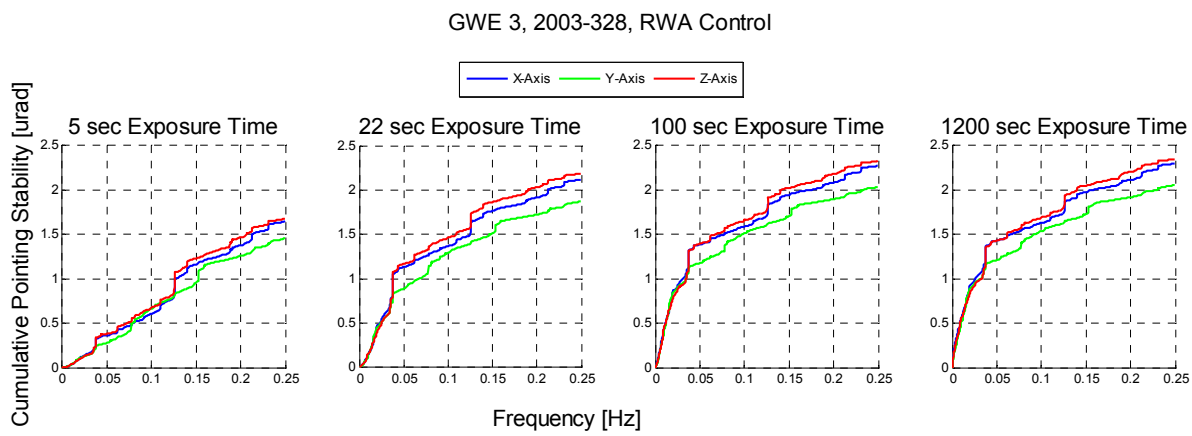

Figure 7. Cumulative Pointing Stability (2-sigma) from the GWE3 Experiment in RWA control for various exposure windows of interest ([5 22 100 1200] sec).

These charts clearly identify the frequencies of major disturbance sources which are responsible for increased jitter. For exposure times longer than 22 seconds, a significant contribution jitter occurs at the low frequencies of 0-40 mHz . Some of this can be explained by the known fundamental frequencies of low-g fuel sloshing (which varies over the life of the mission in accordance to fill fraction). For a 5 second exposure time, the cross-over frequency is ~ 88 m Hz (see Section IIIA). The low-g fuel sloshing frequencies are lower than this cross-over frequency. Hence, fuel sloshing has a small impact on pointing stability performance (for exposure times less than or equal to 5 seconds). The "step" increase in pointing jitter near 0.13 Hz could be due to the vibratory motion of the three RPWS

antennas. The identification of these major jitter sources via the cumulative pointing stability plots is a key advantage of using the RMS stability metric.

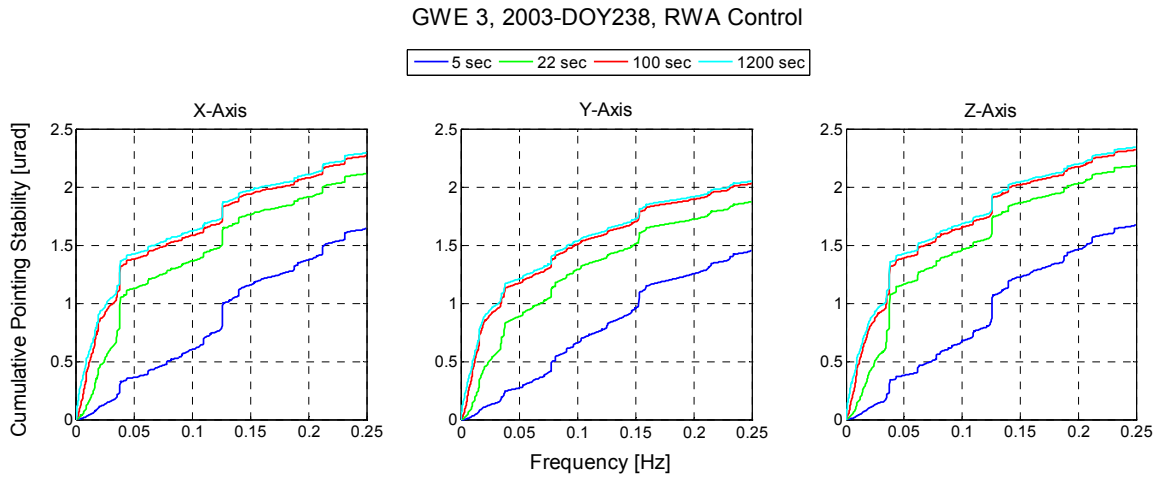

Figure 8. Cumulative Pointing Stability (2-sigma) from the GWE3 Experiment in RWA control for various exposure windows of interest ([5 22 100 1200] sec).

The results in Fig. 8 show the per-axis cumulative pointing stability for a specific experiment in RWA control. From these charts it is clear that both the X and Z-Axis show similar trends of stability disturbances. The Y-Axis pointing stability is consistently better than its X and Z-Axis counterparts. This trend is present in each of the data sets analyzed and is not limited to the example shown above. The per-Axis trends demonstrated above are contrary to a physical interpretation of the system. One would believe based on the spacecraft inertial properties that the X and Y-Axis pointing stability would be very similar. Fig. 9 below shows an enhanced view of the X-Axis pointing stability for the 22 sec exposure window to investigate the details of the frequencies at which disturbances are present.

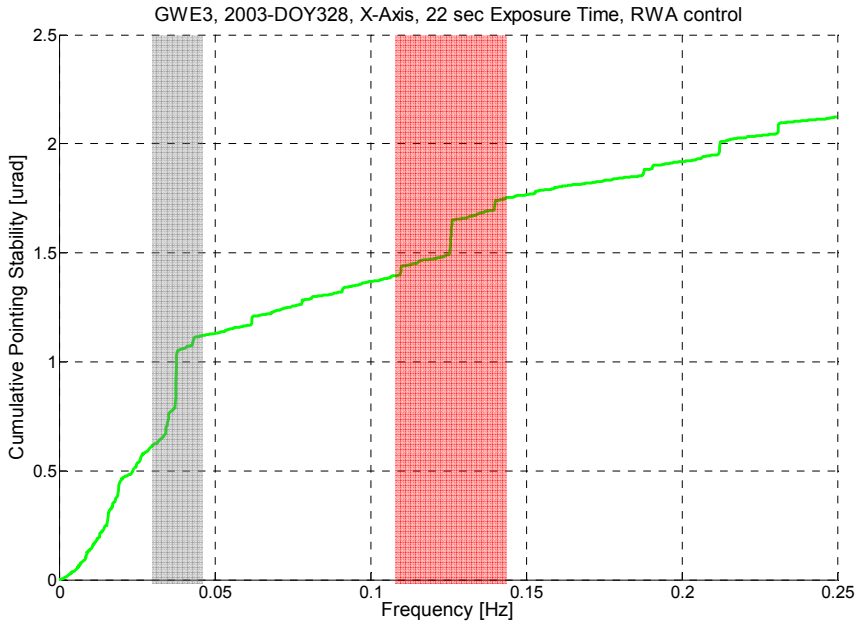

Figure 9. Cumulative Pointing Stability (2-sigma) of the X-Axis on 2003-DOY3288 while in RWA control for a 22 sec exposure window.

In Fig. 9 above, the frequencies at which the pointing stability of the X-axis was most rapidly disturbed are highlighted. The most significant contribution of approximately 0.5 μrad occurs immediately outside of the RWA controller's bandwidth of 0.03 Hz (below this frequency the RWA controller is able to mostly correct for low frequency disturbances). Subsequently, another sudden increase occurs at approximately 0.13 Hz, the designed fundamental frequency of the RPWS antennas. Additional small disturbances are noted in the near region of the RPWS fundamental frequency at approximately 0.11 and 0.14 Hz.

B. Spacecraft Pointing Stability Performance in RCS-controlled Mode

A total of five RCS-controlled events were selected for pointing stability analysis, whose dates ranged from 2004 through 2008. Although RCS was the main control method used for the journey to Saturn, Cassini's tour of the Saturnian system has predominately been executed using RWA control. Throughout the prime mission, RCS control is used for the following events: low-altitude flybys of Titan and Enceladus, orbital trajectory maneuvers, RWA momentum unload events, and a RPWS science experiment that investigates the presence of lightning on Saturn's turbulent atmosphere.

The RCS-based pointing stability performance of Cassini, for the five selected science observations in 2004-2008, is summarized in Table 4. The dependency of the spacecraft pointing stability on exposure time, in log-log scale, is depicted in Fig. 10. Superimposed on these plots is the curve of the RWA-based pointing stability requirement. Note that, for exposure times that are below 60 seconds, RCS-based pointing stability performance meets the RWA-based pointing stability requirements.

Table 4. RMS Pointing Stability, 2σ per axis [μrads]

Mission Phases	Dead-band [mrads]	Exposure Time [s]				Fit Parameters: $\Delta\theta = K\,\Delta T^{\beta}$	
		5	22	100	1200	K	β
				X-axis			
2004-181	2	27	57	121	374	12.6	0.48
2004-360	2	13	45	185	1013	3.6	0.82
2007-115	2	27	61	155	955	8.8	0.65
2007-200	0.5	7.4	27	106	401	2.5	0.76
2008-004	2	32	74	198	1209	10.1	0.67
				Y-axis			
2004-181	2	2.0	2.4	2.9	5.1	1.5	0.16
2004-360	2	19	54	199	1120	5.4	0.77
2007-115	2	55	120	155	1132	21.2	0.53
2007-200	0.5	10	30	92	292	4.0	0.65
2008-004	2	9	28	114	1093	2.0	0.89
				Z-axis			
2004-181	20	138	299	630	1935	65	0.49
2004-360	20	366	795	1686	5215	171.4	0.49
2007-115	20	64	139	382	2867	18.2	0.69
2007-200	0.5	11	40	156	340	4.6	0.67
2008-004	2	16	44	152	883	4.6	0.75

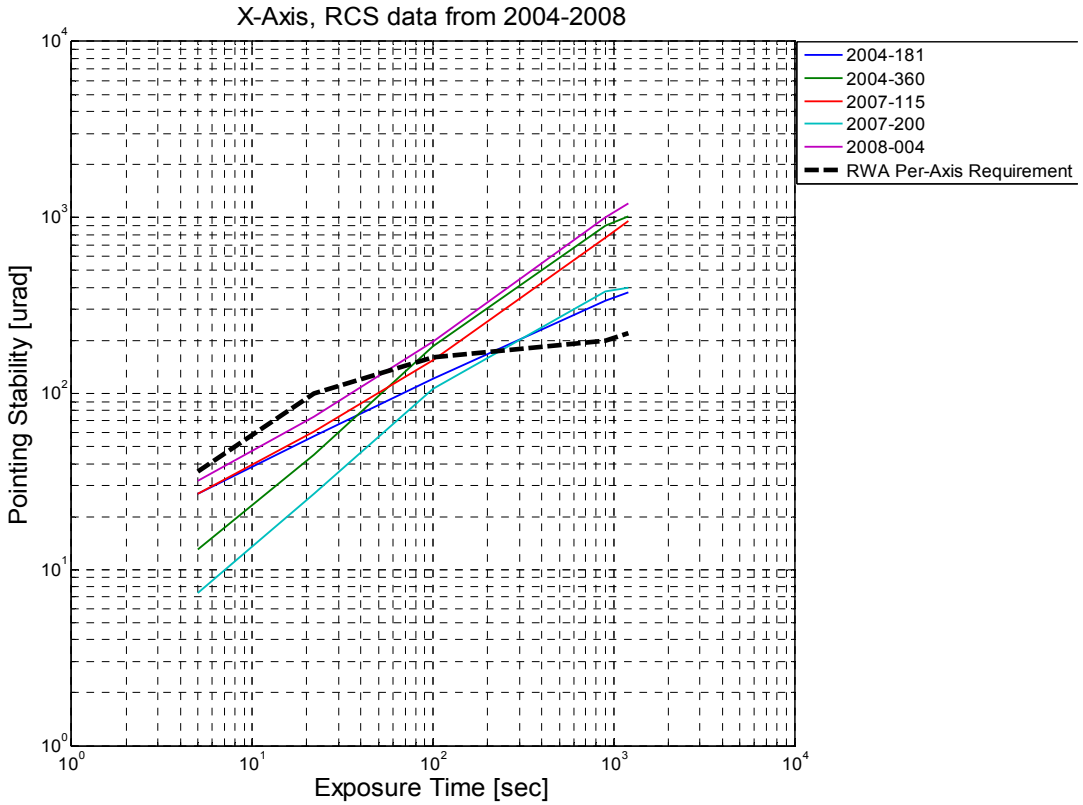

Figure 10. Summary of Spacecraft Pointing Stability (RMS method, 2-sigma) while in RCS-control from 2004-2008 for the X-Axis.

The time histories of the per-axis attitude control errors of an RCS-based science observation on 2004-DOY-181 are depicted in Fig. 11. The dependency of the pointing stability on the exposure time, in log-log scale, is depicted in Fig. 12. The nearly linear relation between the pointing stability ($\Delta\ \theta$), in log scale, and exposure time (ΔT), also in log scale, suggests the following approximate relation: $\Delta\ \theta = K\Delta T^{\beta}$. The values of K and β are given in Table 4. Time histories of the per-axis attitude control errors for four other RCS-based science observations, on 2004-DOY-360, 2007-DOY-115, 2007-DOY-200, and 2008-DOY-004, are given in Appendix B.

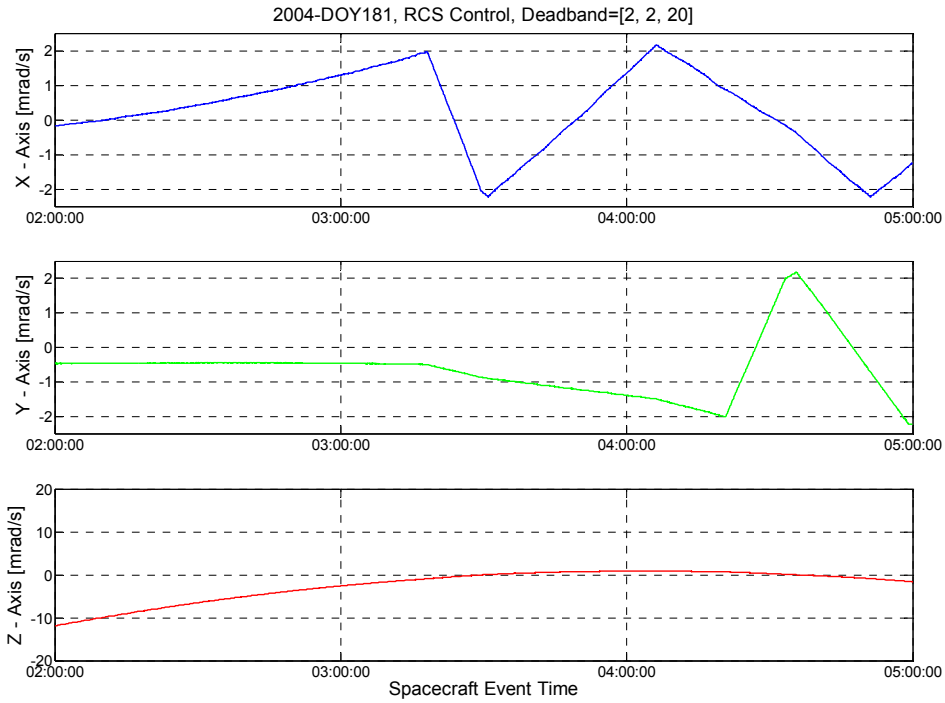

Figure 11. Time Histories of Spacecraft Per-axis Attitude Control Errors [2004-DOY-181]

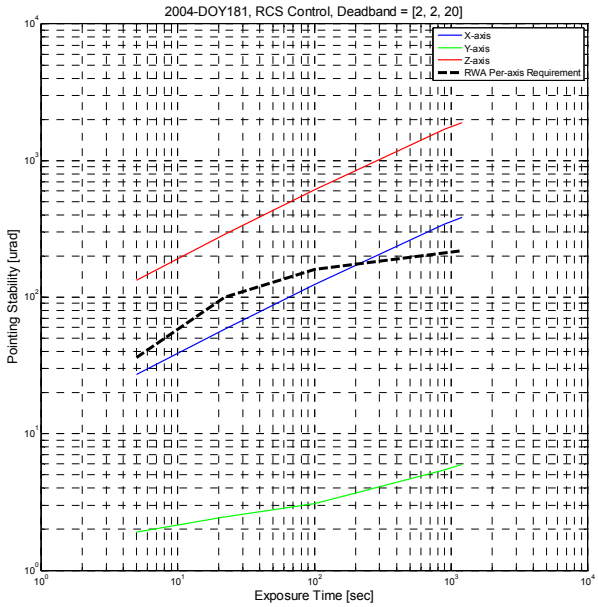

Figure 12. RCS-controlled Spacecraft Pointing Stability [2004-DOY-181, Deadband=(2, 2, 20) mrads]

From results given in Table 4, we observe that:

(1) RCS-based pointing stability performance is strongly related to the commanded dead-band. The smaller the dead-band, the better is the pointing stability. For example, the Z-axis pointing stability (5-s exposure time) of the 2008-DOY-004 observations (with a dead-band of 2 mrads) is about eight times better than that of

2004-DOY-181 observations (with a dead-band of 20 mrads). Similarly, the X-axis pointing stability (for a 5-s exposure time) of the 2007-DOY-200 observations (with a dead-band of 0.5 mrads) is about four times better than that of 2008-DOY-004 observations (with a dead-band of 2 mrads).

(2) From Table 1, the RWA-based pointing stability requirements for exposure times of 5, 22, and 100 s are 36, 100, and 160 μrads, respectively. From Fig. 10, we notice that these pointing stability requirements are generally achievable using RCS control. Pointing stability requirements for an exposure time of 1200 s are harder to achieve with RCS thrusters. Reaction wheels must be employed to achieve these pointing stability requirements.

(3) With per-axis attitude control dead-bands that are 2 mrads or larger, the RCS-based pointing stability increases monotonically with the exposure time: $\Delta\theta = K\Delta T^{\beta}$. As a result, pointing excursion ($\Delta\theta$) could be quite large for long exposure times. If this is unacceptable, one should tighten the attitude control dead-band. For example, note the negative curvature of the pointing stability with respect to exposure time in Fig. B6.

(4) RCS-based pointing stability performance is very un-repeatable. Compare, for example, the Y-axis pointing stability of the 2004-DOY-181 Science observations (with a dead-band of 2 mrads) with those of the 2004-DOY-360 observation (which also has a dead-band of 2 mrads). The behavior of the attitude control limit cycle is functions of many factors such as environmental torque, moment of inertia, and the size of the control thrusters' pulses. At best, one can only put gross bounds on RCS-based pointing stability performance.

(5) The limit cycle behavior of the X-axis attitude control error near 2004-181T03:30:00 (cf. Fig. 11) could be explained as follows. The X-axis rates of the spacecraft before and after reaching the negative edge of the dead-band are Ω_{before} (-5.56e-6 rad/s) and Ω_{after} (+1.95e-6 rad/s), respectively. From these rate estimates, the size of the Z_1 and Z_2 thrusters' pulses (ΔT_{pulse}) fired is:

$$\Delta T_{pulse} \approx \frac{I_{XX}(\Omega_{After} - \Omega_{Before})}{2L_{Thruster} \times F_{Thruster}} \tag{4}$$

Here, I_{XX} is the X-axis moment of inertia of the spacecraft (≈ 8,720 kg-m^2), $F_{Thruster}$ is the magnitude of each thruster (≈0.69 N), and $L_{Thruster}$ is the moment arm of the Z_1 and Z_2 thrusters (≈1.61 m). The size of this particular pair of pulses is 29.5 msec. It is significantly larger than the minimum impulse bit of the thrusters, which is about 7-8 msec. If the RCS controller is properly tuned, the RCS-based pointing stability performance of the spacecraft could be improved.

(6) The Voyager spacecraft attitude was controlled using 0.967-N thrusters (with minimum impulse bit of 15 mNs).[13] The pointing stability requirement of the Voyagers was set at 20 μrad/s while the "goal" was 10 μrad/s (that is, a pointing excursion of 50 μrad over 5 seconds). Nominal attitude control thruster pulse modes used were 10-msec and 60-msec. The 20 μrad/s pointing stability requirement was achievable using the 10-msec pulse mode. Without reaction wheels, this 10-μrad/s goal was difficult to achieve for imaging science during the prime mission. The situation was compounded by the fact that starting and stopping the tape recorder caused adverse limit cycle disturbances. However, in the later part of the extended mission, the operations team throttled the thrusters' on-time way back, ultimately reaching 4 msec during the last few planet encounters. Also, the tape recorder disturbance was controlled by a 'momentum compensation' scheme where thrusters were fired at the right time to cancel the disturbance torques. This FSW modification together with the use of 4-msec thruster pulses contributed to the attainment of the 10 μrad/s pointing stability requirement.[14] From Table 4, we note that the pointing stability performance of Cassini is better than that of Voyager's whenever the attitude controller dead-band is <2 mrads.

(7) The time history of the Z-axis pointing control error of the 2008-DOY-004 Science observations (see Fig. B7 in Appendix) has a distinct behavior. It appears that the thrusters' firings excited a particular spacecraft flexible mode with a frequency of about 2.5 mHz (16 cycles in 1.8 hours). A similar but less obvious excitation is noted in the time history of the Z-axis pointing control error of the 2007-DOY-115 Science observations (see Fig. B3 in Appendix B). It has a frequency of 2.69 mHz (14.5 cycles in 1.5 hours). Both disturbances could be attributed to attitude jitter due to "low-g" sloshing motion of the bipropellant in their tanks. As of 2008, the fill fraction of the tanks are approximately 13% (for both the MMH and NTO tanks), therefore the analytically derived fuel sloshing frequency is in the range of 3-5 mHz.[6] Similar oscillations were also observed in 2001 telemetry on the Z-axis attitude control error (when the fill fractions were higher, at 80%). The oscillation frequency measured was 2.5-2.6 mHz. At a fill fraction of 70%, the analytically derived frequencies are 4-6 mHz. Flight results seem to suggest that the low-g fuel sloshing frequency is 2.5-2.6 mHz regardless of the fill fractions of the tanks.

V. Conclusion

One of the most dramatic demonstrations of the importance of spacecraft pointing stability to mission success happened soon after the launch of the Hubble Space Telescope in 1990. The fine guidance sensors needed to lock Hubble onto guide stars to point it accurately in space were thrown off frequently due to spacecraft pointing jitters that were as large as 1.45 μrads (versus a peak-to-peak requirement of 0.034 μrads, over 24 hr). Cassini carries multiple high-resolution scientific instruments (such as the narrow angle camera) whose proper operations also demand high spacecraft pointing stability. Comprehensive analyses to assess Cassini in-flight pointing stability performance over the past years are performed in this work. Pre-launch, a set of pointing stability requirements is levied on the RWA-controlled spacecraft motion during instrument starting (i.e., zero slew rates). Pointing stability performance computed from ten sets of flight data (spanning 2003-2008) indicates that all the requirements are met with significant margin. Moreover, flight results revealed that most of these pointing stability requirements (that are only applicable when the spacecraft is controlled by the RWA mode) are even met when the spacecraft is under thruster control (especially when the per-axis attitude controller dead-band is tightened to 0.5 mrads).

Overall, the S/C is extraordinarily quiet which underlines the excellence of the overall attitude control design (both software and hardware). Results also confirmed that the measures taken to minimize internal excitation (such as the use of propellant management device to control liquid sloshing, the achieved static and dynamic imbalances of the reaction wheels are three times better than the specifications), as well as the operations use of proper slew rate/acceleration/settling time have been very successful. Lessons learned from both the Cassini AACS design as well as in-flight operations practices should be studied by future space missions if attaining high spacecraft pointing stability performance is critical to mission success.

Acknowledgments

The work described in this paper was carried out by the Jet Propulsion Laboratory, California Institute of Technology, under contract with the National Aeronautics and Space Administration. The authors are grateful to Mr. Vance Haemmerle, a senior member of technical staff, Instrument Software Systems Section of JPL, for many helpful discussions. Any remaining errors of fact or interpretation are of course our responsibility.

References

[1]Jaffe, L. and Herrell, L., "Cassini Huygens Science Instruments, Spacecraft, and Mission," *Journal of Spacecraft and Rockets*, Vol. 34, No. 4, 1997, pp. 509-521.

[2]Abbate, S.F., Armstrong, J.W., Asmar, S.W., Barbinis, E., Bertotti, B., Fleischman, D.U., Gatti, M.S., Glotz, G. L., Herrera, R.G., Less, L., Lee, K.J., Ray, T.L., Tinto, M., Tortora, P., Wahlquist, H.D., "The Cassini Gravitational Wave Experiment", *Proceeding of the SPIE*, Volume 4856, August 23-25, 2002, Waikoloa, Hawaii.

[3]Cassini at Saturn (with 13 papers), *Science*, Volume 307, No. 5713, February 25, 2005, pp. 1222-1276.

[4]Cassini Reveals Titan (with 7 papers), *Science*, Volume 308, No. 5724, May 13, 2005, pp. 978-992.

[5]Lee, Allan Y. and Hanover, Gene, "Cassini Spacecraft Attitude Control System Flight Performance," *Proceedings of the AIAA Guidance, Navigation, and Control Conference, and Exhibit*, San Francisco, California, August 15-18, 2005.

[6]Enright, P. and Wong, E.C., "Propellant Sloshing Models for the Cassini Spacecraft," AIAA Paper 94-3730, 1994.

[7]Macala, G.A., "Design of the Reaction Wheel Attitude Control System for the Cassini Spacecraft," Paper AAS 02-121, AAS/AIAA Space Flight Mechanics Meeting, San Antonio, Texas, January 27-30, 2002.

[8]Wong, E. and Breckenridge, W., "An Attitude Control Design for the Cassini Spacecraft," *Proceedings of the AIAA Guidance, Navigation, and Control Conference*, AIAA, Washington, DC, 1995, pp. 931-945.

[9]Chiang, R.Y., Breckenridge, W.G., and Wong, E., "Self-tuning Thruster Control for Cassini Spacecraft," *Proceedings of the AIAA Guidance, Navigation, and Control Conference*, San Diego, California, July 28-31, 1996.

[10]Barber, T.J. and Cowley, R.T., "Initial Cassini Propulsion System In-flight Characterization", AIAA-2002-4152. Proceedings of the 38th AIAA/ASME/SAE/ASEE Joint Propulsion Conference and Exhibit, Indianapolis, Indiana, July 7-10, 2002.

[11]Lucke, R.L., Sirlin, S.W., and San Martin, A.M., "New Definitions of Pointing Stability: AC and DC Effects," *The Journal of the Astronautical Sciences*, Vol. 40, No. 4, October-December, 1992, pp. 557-576.

[12]Lee, A.Y., Yu, J., Kahn, P., and Stoller, R., "Space Interferometry Mission Spacecraft Pointing Error Budgets," IEEE Transaction on Aerospace and Electronic Systems, Vol. 38, No. 2, pp. 502-514, April 2002.

[13]Cowley, R.T., "Performance of the Voyager Spacecraft Mono-propellant Hydrazine Propulsion System," AIAA/SAE/ASME 17th Joint Propulsion Conference, Colorado Springs, Colorado, July 27-29, 1981.

[14]Savino, J.L., "Voyager – Attitude and Articulation Control Subsystem History," Jet Propulsion Laboratory Inter-Office Memorandum 340-00-045-JLS, September 18, 2000.

APPENDIX A

Table A1. Cassini Narrow Angle Camera Pointing Control Performance

Error Sources	3σ per axis [mrads] X-axis	3σ per axis [mrads] Z-axis	Remarks
Attitude estimation error	0.027	0.01	Flight performance
Star tracker geometric distortion errors	0.3	0.03	Flight calibration results
Calibration error of NAC B/S vector	0.014	0.0023	Flight calibration results
Thermal mechanical instability of the star tracker B/S vector	0.2	0.2	Ground test results
Thermal mechanical instability of the NAC B/S vector	0.07	0.41	Flight performance
Reaction wheel attitude controller error	0.04	0.04	Flight performance
Error of the science target vector (as modeled by an IVP vector in FSW)	0.04	0.04	Ground software capability
Mis-pointing due to IVP timing error	0.037	0.037	Flight hardware limitation
Command resolution error of the Science target vector	0.048	0.048	Flight software implementation error
Error in representing the NAC B/S vector as a fixed body vector in flight software	0.048	0.048	Flight software implementation error
Per-axis Capability	0.380	0.467	Individual error sources are uncorrelated (no common cause)
Radial 99% Capability $\approx 2.575\times RSS(\sigma_X,\sigma_Z)$	0.517		If per-axis errors are fully correlated (Worst case)
Radial 99% Capability $\approx 2.146\times RSS(\sigma_X,\sigma_Z)$	0.431		If per-axis errors are not correlated (Best case)
Radial 99% Requirement	**2.00**		**Requirement is met**

Table A2. Cassini Narrow Angle Camera Pointing Knowledge Performance

Error Sources	3σ per axis [mrads] X-axis	3σ per axis [mrads] Z-axis	Remarks
Attitude estimation error	0.027	0.01	Flight performance
Star tracker geometric distortion errors	0.3	0.03	Flight calibration results
Calibration error of NAC B/S vector	0.014	0.0023	Flight calibration results
Thermal mechanical instability of the star tracker B/S vector	0.2	0.2	Ground test results
Thermal mechanical instability of the NAC B/S vector	0.07	0.41	Flight performance
Telemetry quantization error	0.005	0.005	Flight software implementation error
Error due to timing error	0.002	0.002	Timing error is 10 msec
Per-axis Capability	0.369	0.457	Individual error sources are uncorrelated (no common cause)
Radial 99% Capability $\approx 2.575\times RSS(\sigma_X,\sigma_Z)$	0.504		If per-axis errors are fully correlated (Worst case)
Radial 99% Capability $\approx 2.146\times RSS(\sigma_X,\sigma_Z)$	0.420		If per-axis errors are not correlated (Best case)
Radial 99% Requirement	**1.00**		**Requirement is met**

APPENDIX B

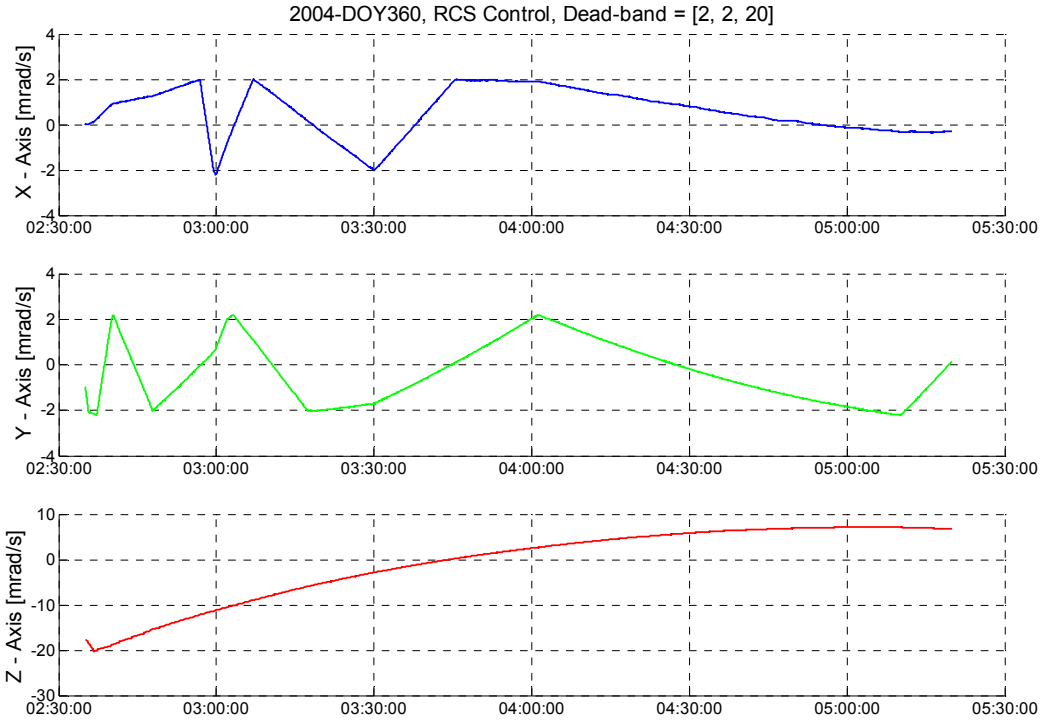

Figure B1. Time Histories of Spacecraft Per-axis Attitude Control Errors [2004-DOY-360].

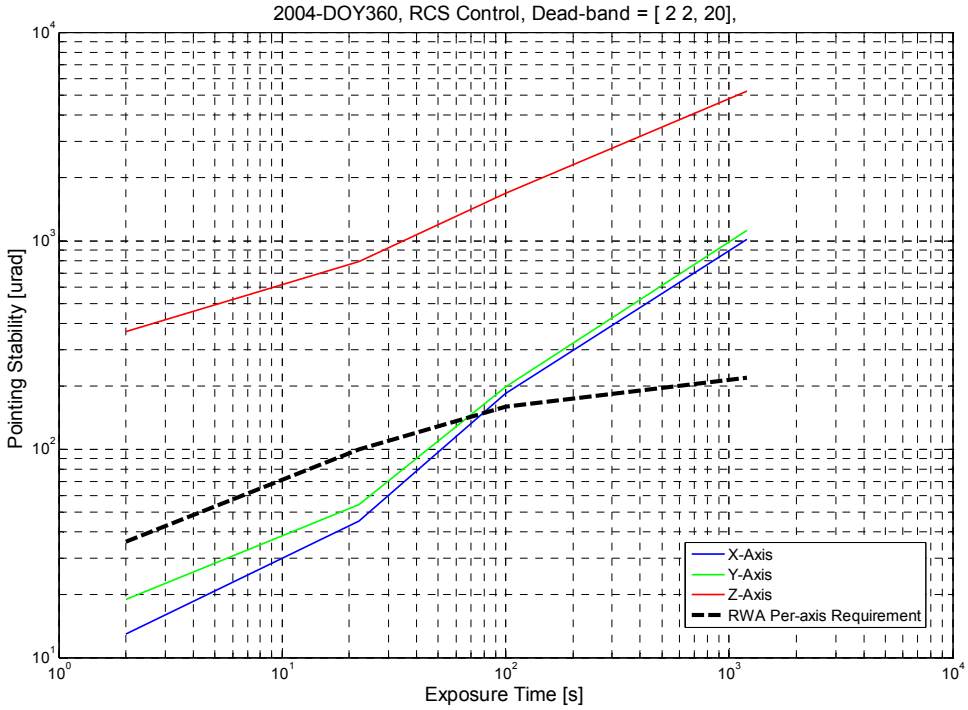

Figure B2. RCS-controlled Spacecraft Pointing Stability [2004-DOY-360] .

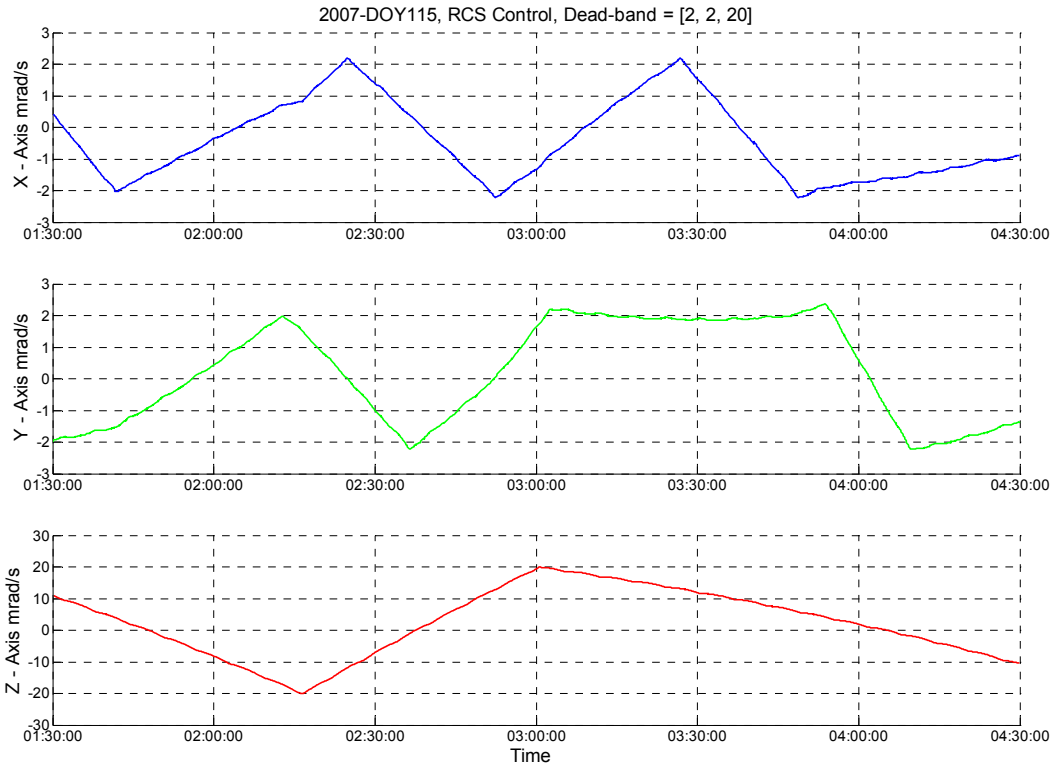

Figure B3. Time Histories of Spacecraft Per-axis Attitude Control Errors [2007-DOY-115].

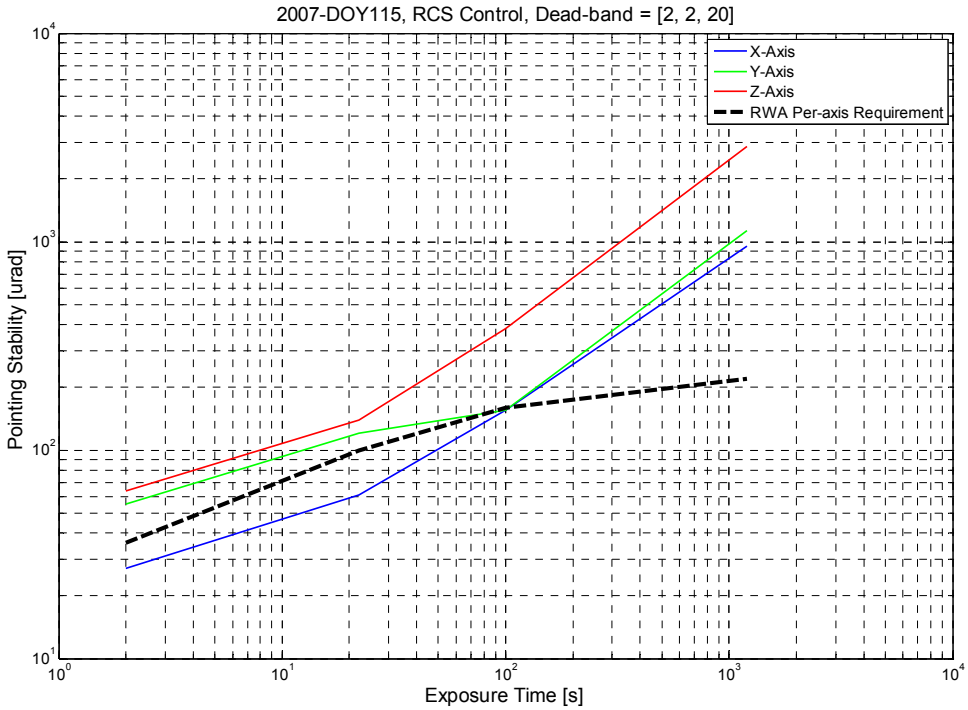

Figure B4. RCS-controlled Spacecraft Pointing Stability [2007-DOY-115].

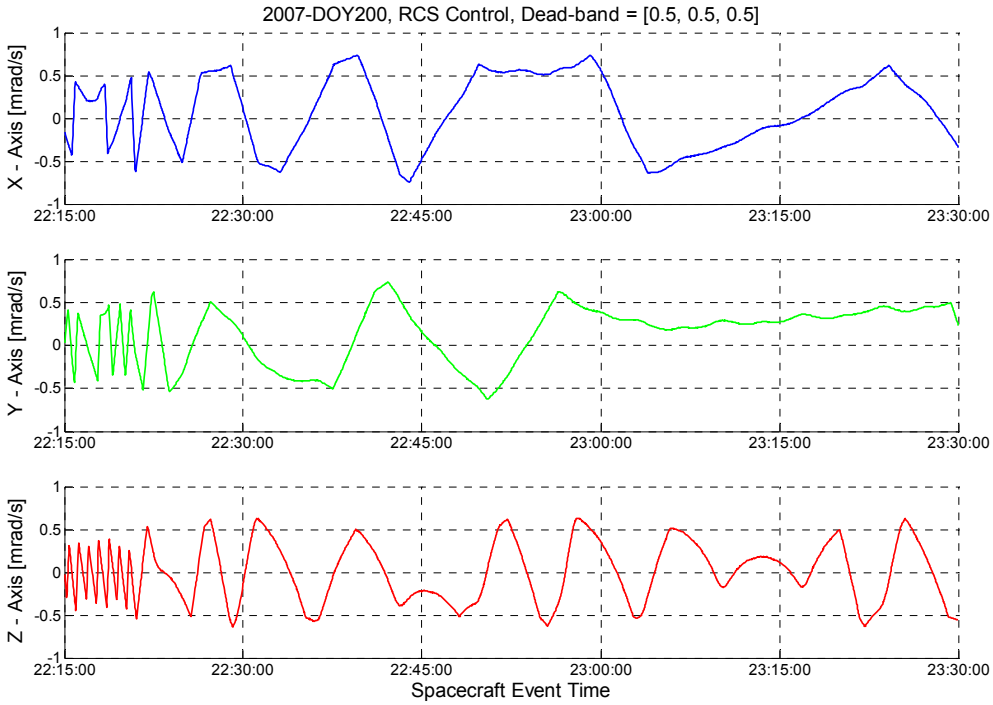

Figure B5. Time Histories of Spacecraft Per-axis Attitude Control Errors [2007-DOY-200].

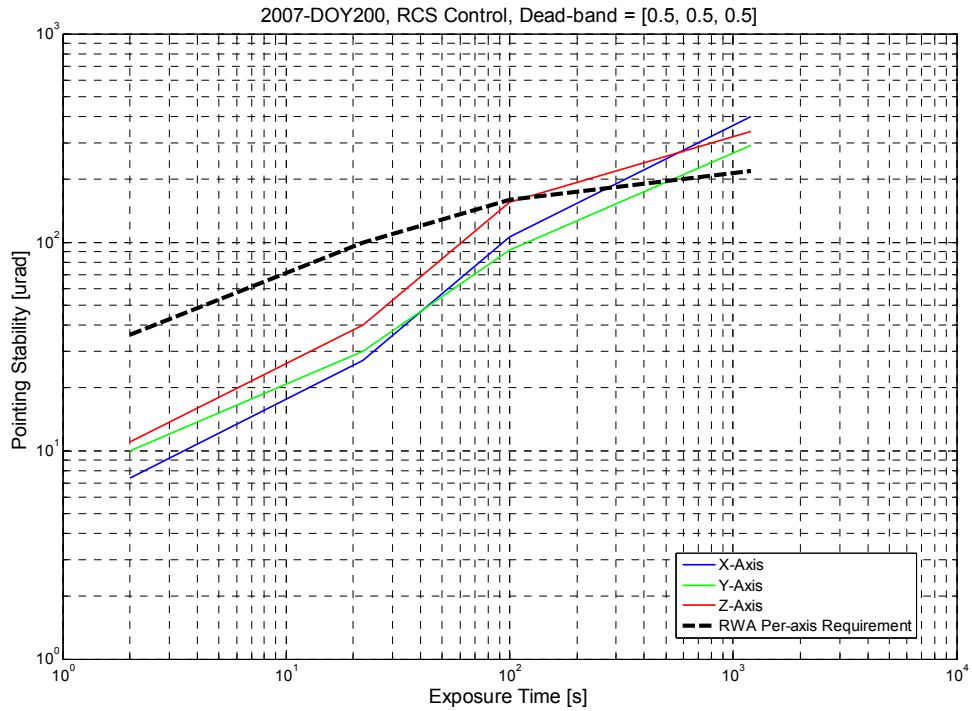

Figure B6. RCS-controlled Spacecraft Pointing Stability [2007-DOY-200] .

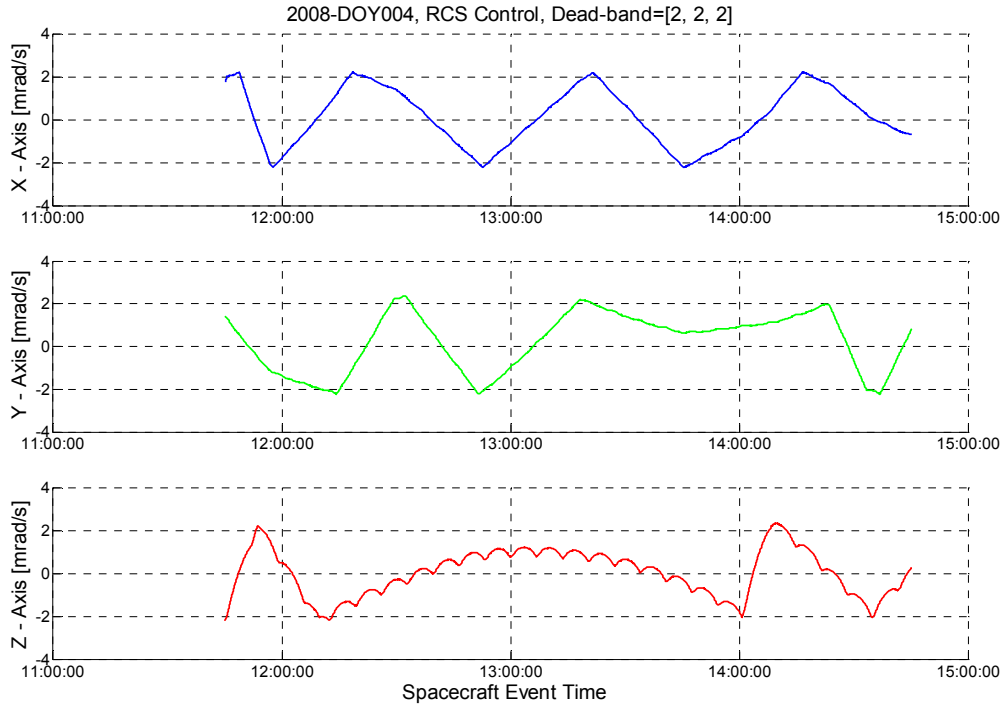

Figure B7. Time Histories of Spacecraft Per-axis Attitude Control Errors [2008-DOY-004].

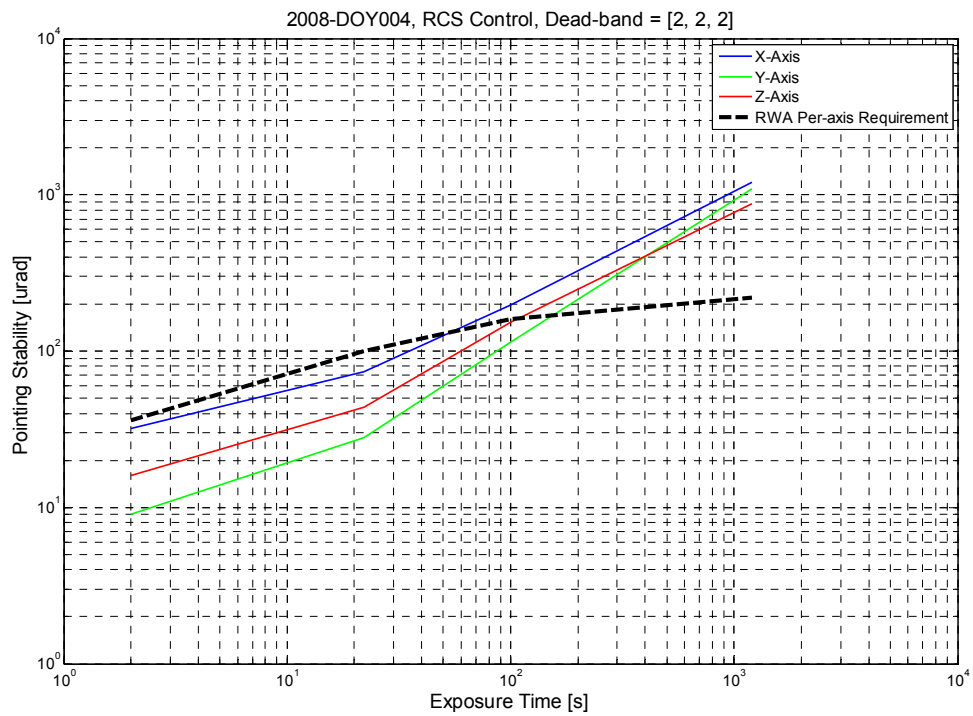

Figure B8. RCS-controlled Spacecraft Pointing Stability [2008-DOY-004].